Suppression of cold air outbreaks over the interior of North America in a warmer climate

Kara Hartig[a] , Eli Tziperman[b]

[b] *Department of Earth and Planetary Sciences and School of Engineering and Applied Sciences, Harvard University, Cambridge, MA*

Corresponding author: Kara Hartig, kara_hartig@g.harvard.edu

ABSTRACT: In spite of the mean warming trend over the last few decades and its amplification in the Arctic, some studies have found no robust decline or even a slight increase in wintertime cold air outbreaks over North America. But fossil evidence from warmer paleoclimate periods indicates that the interior of North America never dropped below freezing even in the depths of winter, which implies that the maintenance of cold air outbreaks is unlikely to continue indefinitely with future warming. To identify key mechanisms affecting cold air outbreaks and understand how and why they will change in a warmer climate, we examine the development of North American cold air outbreaks in both a pre-industrial and a roughly 8×CO_2 scenario using the Community Earth System Model, CESM2. We observe a sharp drop-off in the wintertime temperature distribution at the freezing temperature, suppressing below-freezing conditions in the warmer climate and above-freezing conditions in the pre-industrial case. The disappearance of Arctic sea ice and loss of the near-surface temperature inversion dramatically decrease the availability of below-freezing air in source regions. Using an air parcel trajectory analysis, we demonstrate a remarkable similarity in both the dynamics and diabatic effects acting on cold air masses in the two climate scenarios. Diabatic temperature evolution along cold air outbreak trajectories is a competition between cooling from longwave radiation and warming from boundary layer mixing. Surprisingly, while both diabatic effects strengthen in the warmer climate, the balance remains the same, with a net cooling of about −6 K over 10 days.

SIGNIFICANCE STATEMENT: We compare a pre-industrial climate scenario to a much warmer climate circa the year 2300 under high emissions to understand the physical processes that influence the coldest wintertime temperatures and how they will change with warming. We find that enhanced warming in the Arctic, and particularly over the Arctic Ocean due to the loss of wintertime sea ice, dramatically reduces the availability of cold air to be swept into North America. By tracing these cold air masses as they travel, we also find that they experience the same total amount of cooling in the much warmer climate as they did in the pre-industrial climate, even though many of the individual heating and cooling processes have gotten stronger.

1. Introduction

There is a pressing need to understand trends in modern cold air outbreaks. Despite the overall warming trend in global mean temperature over the past few decades (Arias et al. 2021), there is some disagreement over whether there has been a corresponding warming in North American cold air outbreaks. Some studies have found a decline in wintertime cold air outbreak frequency, intensity, or duration (Hankes and Walsh 2011; Robeson et al. 2014; Screen 2014; Grotjahn et al. 2016; Oldenborgh et al. 2019; Smith and Sheridan 2020), while others have found no robust trend (Walsh et al. 2001; Portis et al. 2006; Westby et al. 2013) or even a slight increase in some regions (Liu et al. 2012; Cohen et al. 2014). If there are mechanisms acting to maintain or even strengthen cold air mass formation in spite of the warming trend, we would do well to identify them so that we can better predict where and when, or even if, they will disappear as warming continues.

Model projections of changes in North American cold air outbreaks over the next few decades are also subject to significant variability, further solidifying the need for a better mechanistic understanding. A study by Vavrus et al. (2006) on the change in cold air outbreaks by the middle of the twenty-first century identified large spatial and inter-model variability, with some regions experiencing a total loss of cold air outbreaks and others no significant change. Identifying the factors responsible for variability would improve confidence in predictions, particularly over the next few decades where models disagree on the trend. A series of studies have implicated a sensitivity to remote sea ice and snow cover conditions (Cohen and Entekhabi 1999; Gong et al. 2003; Vavrus 2007; Cohen et al. 2014; Vavrus et al. 2017), which can vary dramatically from year to year. Preconditioning of the surface that cold air masses pass over can also influence air mass evolution, as a recent history of cold conditions or snow cover can enhance the ability of the land surface to act as a heat sink in the development of the coldest air masses (Ellis and Leathers 1998; Gao et al. 2015; Hartig et al. 2023). Inter-model and spatial variability could also result from competing factors, such as the cooling from longwave radiation balanced by warming from turbulent convection identified in (Hartig et al. 2023), in a competition that has not fully tipped to either side at the observed level of warming.

The question of cold air outbreaks in a warmer climate is also motivated by the Eocene, a warm climate period that persisted from 56 to 34 million years ago. The Eocene presents a challenge to our understanding of cold air outbreaks in a warmer climate due to strong evidence for the complete suppression of below-freezing temperatures over North America. Estimated CO_2 levels during the Eocene range from 600 to over 1,500 ppm, depending on the time period and the proxy used (Beerling and Royer 2011), and the global mean surface temperature was 10 to 16 K higher than in the pre-industrial climate (Inglis et al. 2020). But wintertime continental interiors were much, much warmer than they are today. Fossils of frost-intolerant species from the Eocene, including palms, turtles, and crocodiles, have been found in the central Great Plains and Rocky Mountains of North America (Hutchison 1982; Wing and Greenwood 1993; Markwick 1994; Greenwood and Wing 1995). The presence of these species implies no more than a day at a time below freezing and an absolute minimum temperature above −10°C (Wing and Greenwood 1993; Greenwood and Wing 1995; Hyland et al. 2018) with a cold month mean temperature of at least 4°C (Markwick 1994, 1998) and as high as 13°C (Hutchison 1982). Today, those regions have a cold month mean of −4°C and experience over 100 days per year below freezing with typical wintertime minimums of −30°C to −40°C (NWS 2023), indicating that cold extremes in the Eocene were suppressed by a factor of 2−3 relative to the warming of the wintertime mean.

While multiple lines of fossil evidence point to above-freezing temperatures over Eocene continental interiors, climate models have consistently struggled to simulate conditions that match the proxies. A recent Eocene Model Intercomparison Project noted difficulties matching even the global mean surface temperature over many models in the project (Lunt et al. 2012). Models that can match high- and mid-latitude temperatures produce tropics that are too warm (Shellito et al. 2003), or conversely match the tropics but not higher latitudes (Heinemann et al. 2009). An older CCSM3 model produced reasonable global temperatures but required 4560 ppm CO_2 to do so, which the authors interpret as unrealistically low climate sensitivity rather than a challenge to CO_2 proxies (Huber and Caballero 2011; Caballero and Huber 2013). The previous generation of CESM produced a good match for mean annual temperatures across latitudes in the Eocene (Zhu et al. 2019) but did not look at seasonal means or minimums. The struggle across many models to simulate a feasible Eocene climate suggests that a deeper understanding of the physical processes that enhance or suppress cold extremes will help to identify what is going wrong when models attempt to produce above-freezing continental temperatures in an Eocene-like climate.

In this study, we compare a pre-industrial climate scenario to a much warmer climate to understand the physical processes that influence the coldest wintertime temperatures. The warmer climate corresponds to an extension of a high-emissions scenario out to the year 2300, which is roughly eight times the pre-industrial CO_2 level and falls within the range that produced a good match to an Eocene-era climate in CESM1 (Zhu et al. 2019). Our approach combines a calculation of the high-latitude temperature distribution with a temperature budget along air parcel trajectories to analyze the influence of both initial conditions and diabatic evolution on cold air masses across the two scenarios. We observe a sharp drop-off in the wintertime temperature distribution at the freezing temperature, suppressing below-freezing conditions in the warmer climate and above-freezing conditions in the pre-industrial case. Using air parcel trajectories, we demonstrate a remarkable similarity in both the dynamics and diabatic effects acting on cold air masses across the two climate scenarios. Diabatic temperature evolution along cold air outbreak trajectories is a competition between cooling from longwave radiation and warming from boundary layer mixing of surface sensible heat flux. Surprisingly, while both diabatic effects strengthen in the warmer climate, the net effect remains the same, around -6 K. By identifying the key physical processes influencing cold air outbreaks and how and why they will change in a warming climate, we hope to improve predictions of when and why North American cold air outbreaks can be expected to decline under anthropogenic climate change and demonstrate how Eocene-like climates could have maintained very warm continental interiors.

2. Methods

We approach the evolution of continental cold air outbreaks in a warming climate by comparing a pre-industrial to a warmer climate scenario using the Community Earth System Model, version 2

Scenario	Prescribed SST and Sea Ice	Greenhouse Gases
Pre-industrial	From F1850	CO_2: 284.7 ppm CH_4: 791.6 ppb N_2O: 275.68 ppb F11: 12.48 ppt F12: 0
Year 2300	From years 2290-2299 of the SSP5-8.5 fully coupled run of CESM2-WACCM from CMIP6, with minor corrections based on Hurrell et al. (2008)	CO_2: 2166.15 ppm CH_4: 1070.33 ppb N_2O: 410.72 ppb F11: 333.48 ppt F12: 18.43 ppt

TABLE 1. Details of model setup for the pre-industrial and year 2300 warmer climate scenarios. Pre-industrial GHGs, SST, and sea ice are the same used by the F1850 component set. Year 2300 GHGs are the average over 2290-2300 of the extended SSP5-8.5 scenario (Meinshausen et al. 2020). Corrections to SST and sea ice (Hurrell et al. 2008) for Year 2300: SST$= -1.8$°C if either SST < -1.8°C or ice fraction $\geq 90\%$, ice fraction$= 0$ if < 0 and $= 100\%$ if $> 100\%$, and ice fraction=0 if SST> 4.97°C.

(CESM2). Both scenarios start with a 2000-era climate with prescribed sea surface temperatures and sea ice (the F2000climo component set). For the pre-industrial scenario, we replace the prescribed year 2000 sea surface temperature and sea ice distributions with those of a pre-industrial case, circa 1850, and the atmospheric greenhouse gases with fixed 1850 concentrations. For the year 2300 warmer climate scenario, we prescribe the fixed greenhouse gas concentrations and the sea surface temperature and sea ice distributions using the average over the final decade from the fully coupled run of CESM2 under the SSP5-8.5 high-emissions scenario for CMIP6 extended out to the year 2300 (see Figures S1 and S2 in the supplementary material for surface temperature climatology of this model scenario). Details of both model scenarios can be found in Table 1. The first four years are discarded for spin-up, leaving 50 winters of data that are used in the analysis.

Our methodology for identifying cold air outbreaks, calculating trajectories, and interpolating meteorological variables onto those trajectories follows (Hartig et al. 2023). The reader is directed to that paper for additional detail on the methodology that follows.

We identify cold air outbreaks by sampling from the cold tail of a temperature distribution. To focus on continental cold air outbreaks, we define a sampling region over the interior of North America from 43 to 50°N and from 92 to 104°W, shown as a grey dashed box in Figures 2 and

4. Within the sampling region and for each model scenario, we generate a distribution of the wintertime (December through February) hourly 2-meter air temperature, shown in Figure 1. Cold air outbreaks are identified by randomly sampling from the coldest 5% of that distribution. To avoid double-counting a given air mass, we impose the additional constraint that samples must be at least three days apart from each other. Under this constraint, we sampled 400 cold air outbreaks in the pre-industrial scenario and 500 in the warmer climate.

We use air parcel backtracking to follow the evolution of air masses resulting in cold air outbreaks over North America. Each cold air outbreak identified with the method above is used to initialize a 10-day backwards trajectory, starting 100 meters above the ground at the location within the sampling region corresponding to the event. We perform the trajectory calculations with HYSPLIT, a trajectory and dispersion model developed by NOAA's Air Resources Laboratory (Draxler and Hess 1998, 1997; Draxler 1999; Stein et al. 2015), with two custom modifications to improve data resolution described in detail in (Hartig et al. 2023). The trajectory calculations (resulting in latitude/longitude/altitude vs. time) are performed using hourly wind and other meteorological fields from the CESM2 model scenarios. Meteorological quantities are then interpolated onto the latitude, longitude and altitude of the air parcel for each hour along the trajectory.

Of particular interest in this study are the factors influencing temperature change within the model. The model temperature tendency at each gridpoint $\dot{T}$ can be decomposed as,

$$\dot{T} = \dot{T}_{physics} + \dot{T}_{dynamics} + \dot{T}_{fix}, \tag{1}$$

where $\dot{T}_{physics}$ is the diabatic tendency from the model physics while $\dot{T}_{dynamics}$ is calculated by the model's dynamical core and accounts for advection, adiabatic compression and expansion, and the divergence damping (which is expected to be small). The term $\dot{T}_{fix}$ is a very small energy correction, typically $< 10^{-4}$ K/hr, that ensures the conservation of global energy.

Ultimately, we want to separate out the diabatic temperature tendencies $\dot{T}_{physics}$ from the advective and adiabatic terms $\dot{T}_{dynamics}$. To remove the advective component of the model dynamics term, we use a Lagrangian reference frame by considering temperature tendencies along an air parcel trajectory instead of at a fixed point. To remove the adiabatic component, we transform from temperature to dry static energy, which is conserved under adiabatic motion,

$$DSE = c_p T + gz, \tag{2}$$

where T is temperature, g is gravitational acceleration, c_p is the specific heat of air, and z is geopotential height ($z = 0$ at sea level). Whenever we refer to dry static energy throughout the rest of this paper, it is divided by the specific heat of air c_p to give units of temperature.

These transformations leave us with a dry static energy budget along air parcel trajectories consisting of temperature tendencies from distinct physics processes,

$$\begin{aligned} D\dot{S}E &= \dot{T}_{physics} \\ &= BL + DP + LW + SW + VD + GW + \dot{T}_{fix} \\ &\approx BL + DP + LW, \end{aligned} \tag{3}$$

where BL is boundary layer mixing, DP is deep convection, LW is longwave radiation, SW is shortwave radiation, VD is vertical diffusion, and GW is gravity wave drag. In the final line, we drop the last four terms, which are consistently over an order of magnitude smaller than the leading three terms in the troposphere over North America during winter. We also note that the tendencies due to boundary layer mixing BL and deep convection DP are shorthand for a partitioning of the moist processes temperature tendency within the atmosphere model, $\dot{T}_{moist\,processes} = BL + DP$, and are used as umbrella terms for a collection of processes. BL refers to the temperature tendency from the CLUBB parametrization (Golaz et al. 2002; Bogenschutz et al. 2013) and includes boundary layer turbulence, shallow convection, and latent heat from liquid cloud formation and evaporation, while DP is the remainder of moist processes and includes deep convection, cloud microphysics, and re-evaporation of rain and snow.

By integrating over time along a trajectory, we formulate a Lagrangian dry static energy budget that decomposes the total change in dry static energy of the air parcel into the diabatic contributions

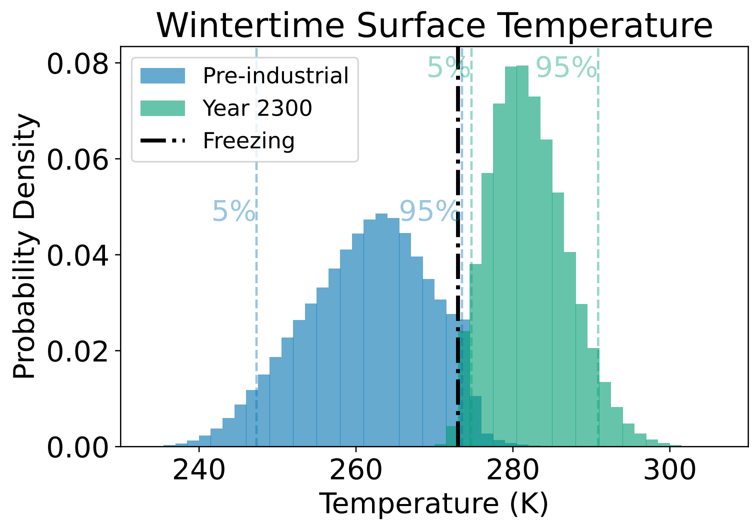

FIG. 1. Narrowing of the wintertime surface temperature distribution in warmer climates. Distribution of hourly 2-m surface air temperature over the interior of North America (see grey dashed box in Figure 2) between December 1st and February 28th over 50 simulated winters. The Pre-industrial scenario is shown in blue and the Year 2300 scenario in green. For reference, the 5th and 95th percentiles are marked by colored dashed lines and the freezing temperature (273 K) by a black dashed line.

from distinct model physics processes,

$$\begin{aligned} \Delta DSE &\approx \int (BL + DP + LW)\, dt \\ &= \int \dot{T}_{physics} dt. \end{aligned} \tag{4}$$

3. Results

We begin with overall changes to the wintertime temperature distribution over the interior of North America between a pre-industrial and a much warmer climate in section a. The effect of changes to the climatology and geographical distribution of source regions for cold air masses is considered in section b, while the role of diabatic processes acting on those air masses as they are swept over the interior of North America are covered in section c.

a. Narrowing of the wintertime temperature distribution

We begin with a consideration of the changes to the wintertime temperature distribution itself when moving from a pre-industrial climate to a much warmer climate. Figure 1 shows the Dec-Jan-Feb distributions of hourly 2-m air temperature over the sampling region in the interior of North America in the pre-industrial (blue) and year 2300 (green) modeled climate scenarios. In a warmer climate, the wintertime temperature distribution not only warms but also becomes narrower, with a cold tail that barely drops below freezing. The freezing temperature itself (vertical black line in the figure) helps to illustrate the dramatic change between the two scenarios: the wintertime temperature in this region almost never rises above freezing in the pre-industrial scenario and almost never drops below freezing in the warmer climate. There is, in fact, a particularly abrupt drop in both scenarios right around freezing. We argue that this suppression of temperature extremes around the freezing temperature is a result of the energy consumed by the latent heat of freezing in soil water. Using a range of volumetric heat capacities from 1.5×10^6 to 3×10^6 J/m^3·K to account for variations in soil type and moisture content (Abu-Hamdeh 2003), we find with a back-of-the-envelope calculation (detailed in the supplementary materials and Figure S3) that the top 10 cm of soil contains more than enough water for the latent heat of freezing to entirely offset the surface energy imbalance that accumulates over the two days leading up to a typical cold air outbreak. Near-surface air temperatures would thus stall out at the freezing temperature as energy is diverted to melt or freeze water in the soil, reducing the prevalence of above-freezing temperatures in the pre-industrial climate and of below-freezing temperatures in the warmer climate. We note that this mechanism assumes efficient energy exchange between the soil surface and the lowest layers of air as well as within the soil to transmit the latent heat of freezing up into contact with overlying air, either of which might be exaggerated in the model to compensate for vertical discretization. Further work is required to confirm that the control that the phase change of soil water appears to have on near-surface air temperatures in CESM also operates in the real climate.

The increase in average wintertime temperature between the pre-industrial period and our year 2300 scenario, as demonstrated by Figure 1, is unsurprising. Between a CO_2 concentration almost eight times that of the pre-industrial case and a total loss of Arctic sea ice, a wintertime mean temperature of 282 K (9°C, an increase of 21 K relative to pre-industrial) for the warmer climate is in line with paleoclimate proxies for the Eocene warm climate period (56–34 Myr), when frost-intolerant species such as crocodiles and palm fronds populated the interior of North America (Hutchison 1982; Wing and Greenwood 1993; Markwick 1994; Greenwood and Wing 1995; Hyland et al. 2018). What is more interesting, at least from a dynamical perspective, is the change in temperature extremes. The 5th percentile of hourly temperature has increased by 27 K between the two scenarios, or 1.3 times the increase in the wintertime mean, while the 95th percentile has increased by only 0.8 times the mean. The amplified warming of cold extremes is consistent with (Cronin and Tziperman 2015) who present a low cloud mechanism for suppressing cold air formation in a warmer climate. In our modeled scenarios, cold air outbreaks have indeed warmed by more than both the mean and hot extremes; understanding why this happens is a central goal of this paper.

To understand why wintertime temperature extremes are suppressed in a warmer climate, we consider changes in temperature in terms of two interrelated factors, (1) the location and temperature of source regions for cold air masses and (2) diabatic forcings acting on those air masses as they travel. The diabatic forcings include solar and infrared radiation, latent heating from the condensation or evaporation of water, and boundary fluxes like the surface sensible heat flux. In the shift to a warmer climate, changes to CO_2 concentration, atmospheric moisture, clouds, land cover, and precipitation can alter the diabatic forcings acting on an air mass as it travels. Source regions, on the other hand, can be thought of as setting an initial state of temperature and moisture that both is acted upon by and influences diabatic forcings. In our study of cold extremes over the interior of North America, we will therefore consider both changes to the climatology of source regions and changes to diabatic temperature tendencies along air mass trajectories in our attempt to tease out the causes of cold air suppression in a warmer climate.

b. A warmer and less stable source region

Beginning with temperature changes in source regions, we note the dramatic reduction in frequency of below-freezing days in Arctic source regions between the pre-industrial and the year 2300 scenarios illustrated in Figure 2. The coldest temperatures over the interior of North America in the modern climate usually result from anomalous advection of air masses out of Arctic regions, where dryness and low temperatures set a cold initial state that is enhanced or maintained as these air masses cross the continent (Walsh et al. 2001; Cellitti et al. 2006; Portis et al. 2006; Vavrus et al.

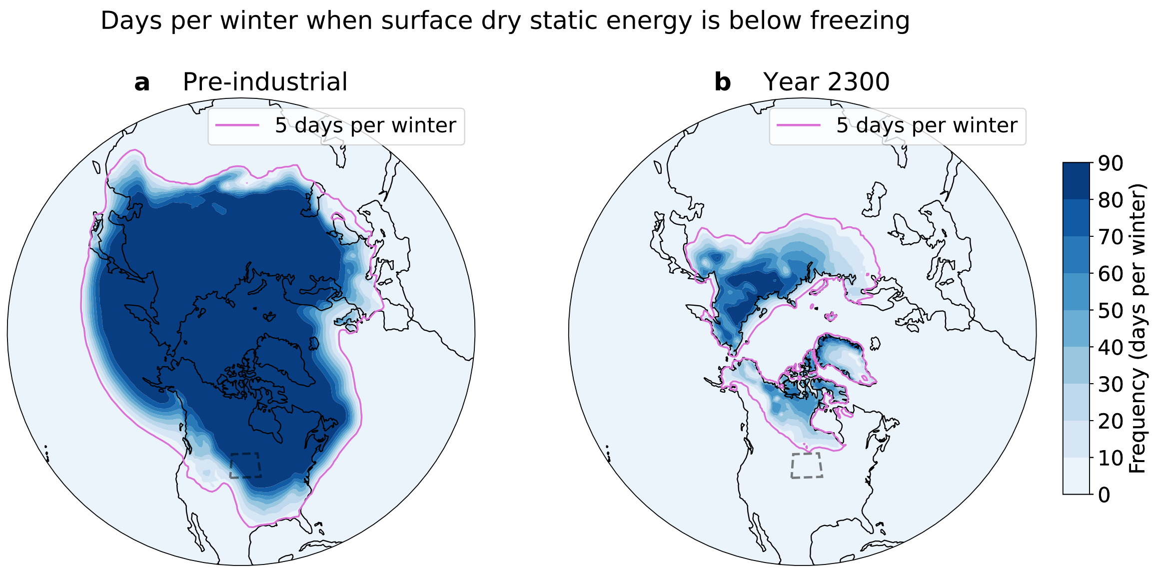

FIG. 2. Reduction in area below freezing over continental cold air source regions in a warmer climate. Number of days per winter (December through February, averaged over 50 simulated winters) when the average daily surface dry static energy is above freezing. A solid contour has been included in fuchsia marking five days per winter to better demarcate the low-frequency regions. Note that, for this figure, dry static energy has been adjusted to a reference height of 510 m instead of sea level such that it reflects the temperature the air parcel would be if raised or lowered adiabatically to the average surface height over interior North America (grey dashed box in figure).

2006; Kolstad et al. 2010; Hankes and Walsh 2011; Smith and Sheridan 2018; Hartig et al. 2023). By using surface dry static energy relative to a reference height of 510 m instead of temperature, we are actually looking at the temperature these air masses would have after the adiabatic compression or expansion due to vertical motions that would accompany advection into the interior of North America (specifically, the grey dashed box in the figure, which has an average surface elevation of 510 m; for the same figure using surface air temperature, see Figure S4 in the supplementary materials). We leave the consideration of diabatic processes for the second half of this paper. Figure 2 shows a nearly order-of-magnitude reduction in the frequency of below-freezing days over the northernmost parts of North America and a total loss of such conditions over the newly exposed Arctic Ocean in the year 2300 scenario. We also note that Figure 2 is, if anything, a conservative estimate of the availability of below-freezing air masses for North America. Adiabatic compression will heat any air mass brought to the surface from aloft, so if air masses destined for North America

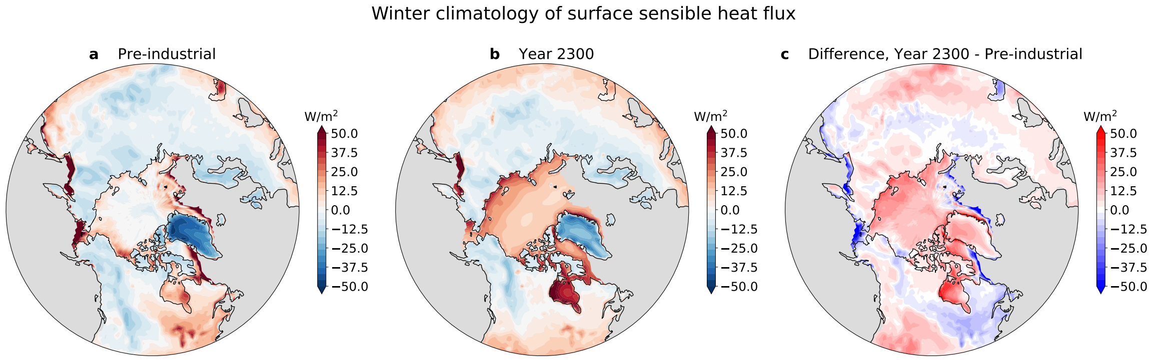

FIG. 3. Changes in surface sensible heat flux with the disappearance of Arctic sea ice. Wintertime climatology over 50 simulated winters of surface sensible heat flux, masked in grey to exclude regions with open ocean in the pre-industrial period (both sea ice and land fraction less than 50%). Includes Pre-industrial model climatology (left), Year 2300 (center), and the difference between the two scenarios (right). Positive values indicate heat flux from the surface into the atmosphere.

are sourced even a few hundred meters above the surface, then the heating from subsidence can partly or fully counteract the below-freezing initial temperature.

The biggest change in the year 2300 climate scenario other than the increase in CO_2 is the complete loss of Arctic sea ice and subsequent dramatic changes in heat and moisture fluxes in the Arctic. With the ocean surface fully exposed, surface sensible heat fluxes into the atmosphere increase by tens of W/m^2 relative to the pre-industrial climate, as shown in Figure 3. The loss of insulating sea ice makes near-surface air over the Arctic Ocean warmer rather than colder than bordering continental air, and provides a heat source to any air masses passing over it. For instance, while a large number of below-freezing days persist over Siberia in the warmer climate (Figure 2), any cold air masses originating there would need to pass over open ocean to reach North America, where they would be subject to significant positive surface heat fluxes (Figure 3).

Given the dramatic changes in the distribution of cold air in the northern high latitudes discussed above, we begin our air parcel trajectory analysis with an investigation into the extent to which the geographical distribution of source regions may have shifted in the warmer climate. After identifying cold air outbreaks over the interior of North America (grey dashed box), we calculate a 10-day back trajectory for each event (see section 2 for details). The resulting trajectory paths are shown in Figure 4 for both the pre-industrial and year 2300 model scenarios. While a larger

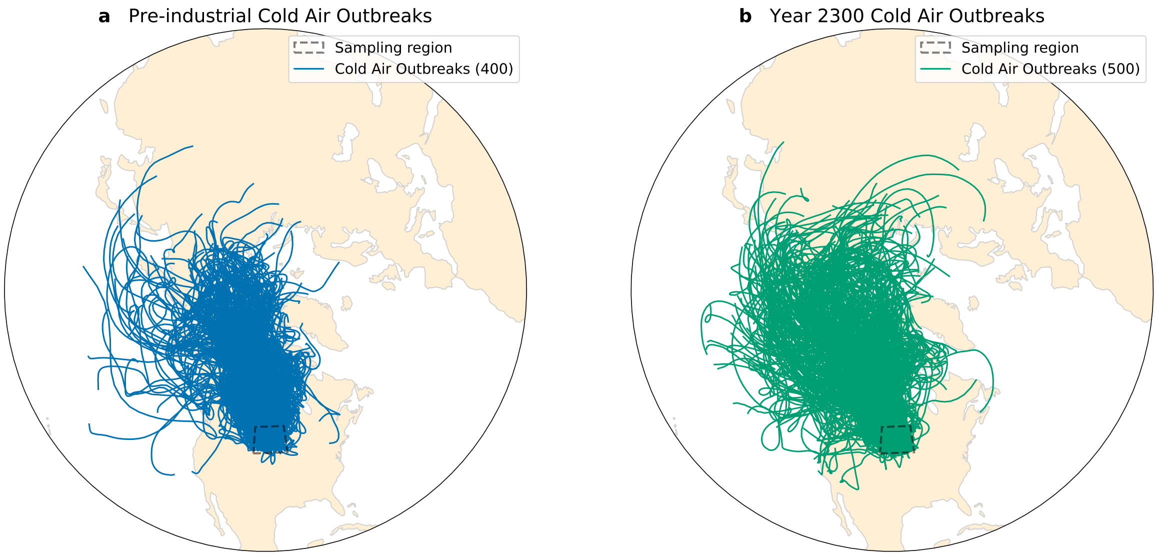

FIG. 4. Back trajectories of cold air outbreaks. Each line represents a 10-day back trajectory initialized from a cold air outbreak identified in the pre-industrial (left, blue) or year 2300 (right, green) model scenario. The cold air outbreaks used to initialize each trajectory were identified by randomly sampling 400 times (for pre-industrial scenario) or 500 times (for year 2300 scenario) from the coldest 5% of hourly 2-m air temperatures over 50 simulated winters within the sampling region (black dashed box); see section 2 for more details on the sampling method.

fraction of cold air outbreaks pass over the Pacific Ocean in the year 2300 case, it is remarkable how little the source region and air mass trajectories have changed overall. Over half of all trajectories still pass over the Arctic Ocean in the warmer climate scenario, even in spite of the positive heat fluxes (Figure 3) and dramatically reduced availability of below-freezing days there (Figure 2).

Another climatological change in the northern high latitudes between the two climate scenarios becomes obvious in the vertical temperature distribution, shown in Figure 5 as a composite of air columns averaged over all cold air outbreak trajectories. In the pre-industrial climate, there is a persistent near-surface temperature inversion in the winter high latitudes. The presence of the inversion results in cold air outbreak trajectories that stay close to the ground; these near-surface air masses are actually colder than the air aloft, and low or even negative sensible heat fluxes along the trajectory paths (Figure 3) keep these air masses cold as they travel out of the Arctic. In the warmer climate, the temperature inversion has disappeared in favor of a steady decline in temperature with height. Positive surface sensible heat fluxes over the Arctic (Figure 3) in the

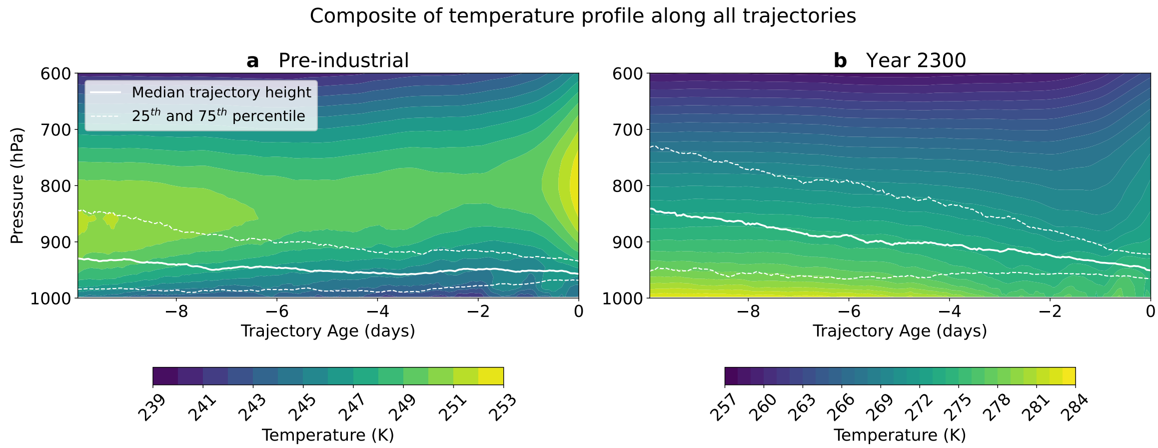

FIG. 5. Loss of the surface temperature inversion along cold air outbreak trajectories. Composites of the vertical temperature profile over all cold air outbreak trajectories (colored lines in Figure 4) in the pre-industrial (left) and year 2300 (right) model scenarios. The x-axis is the time along the trajectories in days, where day 0 represents the occurrence of the cold air outbreak in the sampling region. The spread of air parcel trajectory heights within these composite profiles is indicated by a solid white line for the median height and dashed white lines for the $25^{th} - 75^{th}$ percentile range across all trajectories. Note that the contour range is different between the two figures, but the contour spacing is the same (1 K).

first half of the trajectories and cooler temperatures aloft than at the surface mean that cold air outbreak air masses originate higher up in the atmosphere in the warmer climate than they do in the pre-industrial case.

c. Enhanced diabatic heating and cooling

With the initial temperature determined by the climatology in source regions, diabatic heating and cooling provide the final piece to determine temperature evolution as those air masses travel into the mid-latitudes. If there is net diabatic heating along a trajectory, it can offset the initially low temperatures of the Arctic air parcel and suppress cold air formation. Conversely, if there is net diabatic cooling, the air mass can become even colder as it travels into the mid-latitudes, so diabatic sources are critically important in determining the development of cold air outbreaks.

Using a Lagrangian air parcel perspective, we can separate the temperature tendency due to diabatic forcings from the advective and adiabatic components. We take advantage of the way that CAM6 separates temperature tendency into distinct physical processes to decompose diabatic temperature evolution into five terms: boundary layer mixing, deep convection, longwave radiation, shortwave radiation, and gravity wave drag. The last two terms, shortwave radiation and gravity wave drag, are more than an order of magnitude smaller than the other components, so we leave them out of the analysis that follows (see Figure S7 in the supplementary materials for all components). Additionally, the tendencies due to boundary layer mixing and deep convection are each shorthand for a collection of processes within the atmosphere model that are explained in more detail in section 2. We interpolate each temperature tendency onto the air parcel trajectories and then integrate along each trajectory to get a distribution over all trajectories of the ten-day diabatic temperature tendency attributable to each physical process, shown in Figure 6.

We note a crucial balance in the diabatic temperature evolution of cold air masses in both the pre-industrial and year 2300 climate scenarios. In both scenarios, diabatic temperature evolution is almost entirely dominated by a competition between cooling from longwave radiation (Figure 6a) and warming from boundary layer mixing (Figure 6b). The key difference between the two scenarios is that both processes become more intense in the warmer climate; longwave cooling of the air mass is actually stronger in the warmer climate, while boundary layer mixing provides more heating at the parcel level. The two processes nearly cancel out when averaged over all trajectories, but the spread across trajectories is large (see Figure 6d), indicating that individual trajectories may experience large diabatic temperature change in either the positive or negative direction. For reference, we note that the 5th percentile of surface temperature is only 7.3 K below the winter average temperature of 282 K over the interior of North America in the year 2300 scenario (Figure 1), and the surface temperature in source regions is only below freezing a few days every year (Figure 2). And while the *average* diabatic temperature change is just a few degrees, the large spread in Figure 6 means that most trajectories in fact have a non-zero diabatic temperature change. This means that the diabatic temperature change, which is commonly 10 or 20 K over ten days according to Figure 6, is sufficient to entirely determine whether an Arctic air mass becomes a cold air outbreak in the year 2300 scenario, and to a lesser extent in the pre-industrial scenario as well.

Two questions naturally arise from the changes in diabatic temperature contributions between the pre-industrial and year 2300 scenarios in Figure 6a and 6b: why does boundary layer mixing lead to more heating in the warmer climate? And why is longwave cooling more intense?

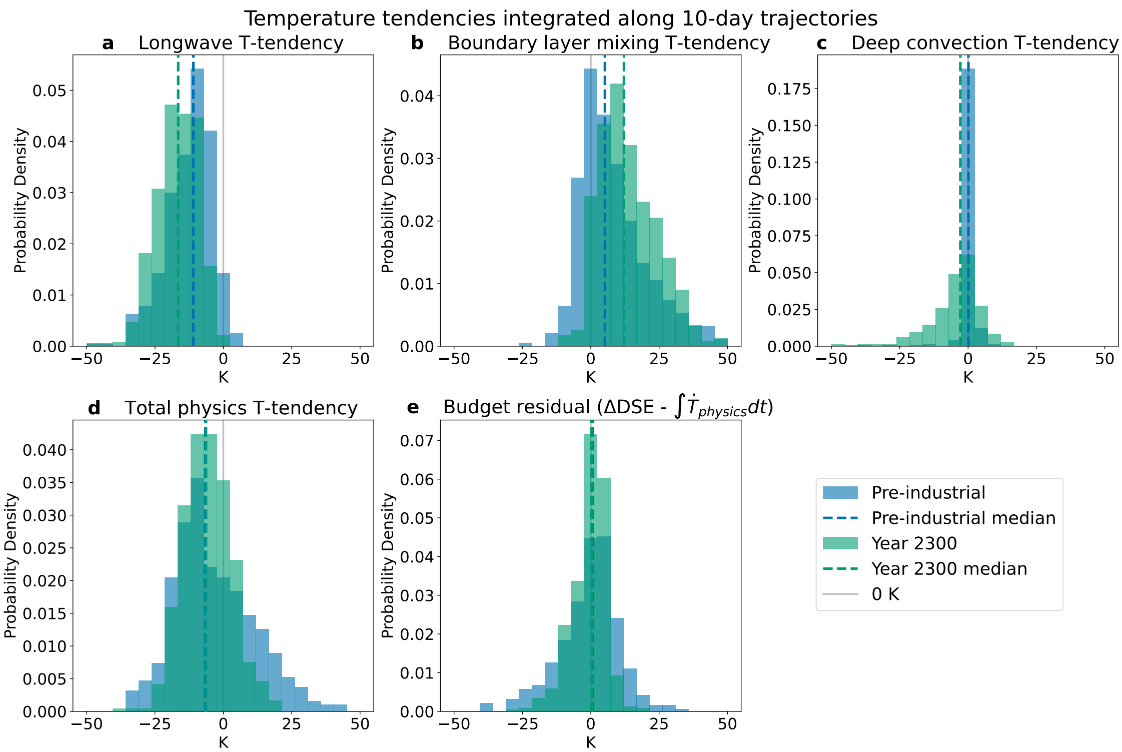

FIG. 6. Contributions to diabatic temperature evolution along cold air outbreak trajectories. Each histogram shows the distribution across all trajectories of the cumulative temperature contribution of a specific model physics process, found by integrating the hourly temperature tendency along each 10-day trajectory. The three largest contributions to the total diabatic temperature evolution are shown along the top row: longwave radiation (a), boundary layer mixing and latent heat of condensation/evaporation (b), and deep convection and cloud microphysics (c). The bottom row shows the total diabatic temperature tendency (d) and the total budget closure residual (e; $\Delta DSE - \int \dot{T}_{physics} dt$), which measures how well changes in dry static energy match up with the diabatic temperature tendencies given by the model.

There are two key changes in the warmer climate that can facilitate both heating from boundary layer mixing and cooling from deep convection. The loss of the surface temperature inversion (Figure 5) removes a major barrier to convection, allowing both shallow and deep convection to proceed more readily. The increase in surface fluxes of heat (Figure 3) and moisture into the atmosphere inject more heat into the boundary layer and can help fuel convection. Mixing in the boundary layer redistributes those surface fluxes throughout the boundary layer, leading to heating as shown in Figure 7, while deep convection transports surface heat upwards into the mid-troposphere, leading to cooling in the boundary layer and heating aloft (see Figure S8 in the

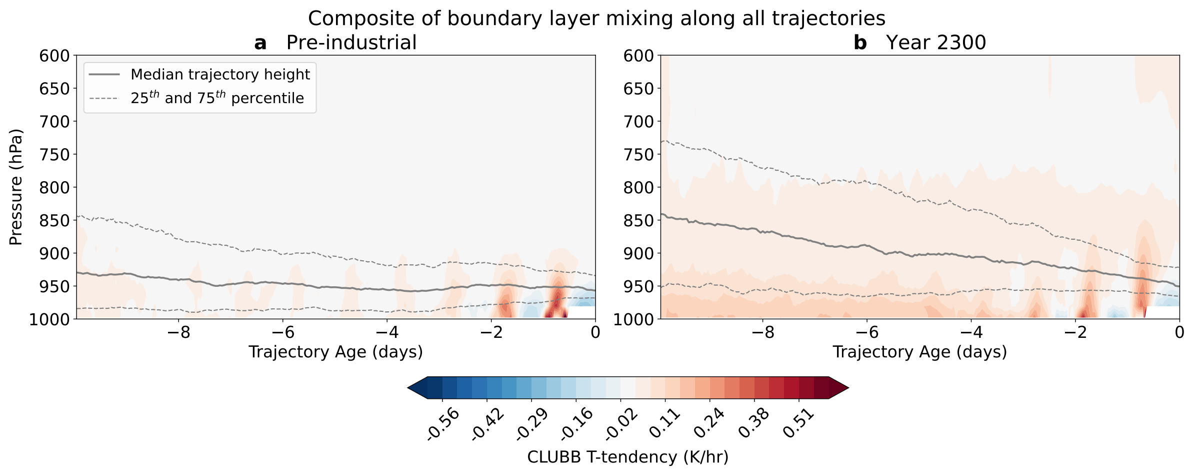

FIG. 7. Boundary layer mixing brings more heat higher up in the warmer climate. Composites of the boundary layer mixing temperature tendency profiles (shaded contours) over all cold air outbreak trajectories (colored paths in Figure 4) in the pre-industrial (left) and year 2300 (right) model scenarios. Grey lines mark the median (solid) and 25^{th}–75^{th} percentile range (dashed) of trajectory heights across all trajectories.

supplementary materials for deep convection profiles). Evidently, more heat is distributed within the boundary layer where most of these trajectories reside than is carried aloft (cooling from deep convection in Figure 6c for most trajectories is weaker than heating from boundary layer mixing in 6c), but both processes are enhanced by the loss of the near-surface stable layer and increased surface heat fluxes in the migration from a pre-industrial to a warmer climate.

Longwave radiation is the only significant source of diabatic cooling that remains in the warmer climate. Deep convection is just −5 K over ten days on average in the warmer climate, while boundary layer mixing becomes almost strictly positive. Continental cold air outbreaks, therefore, rely almost entirely on longwave cooling to make or keep Arctic air masses cold into the mid-latitudes. The intensification of longwave cooling in the warmer climate is therefore crucial to identifying how cold air outbreaks respond to warming.

We find that the increase in longwave cooling is due primarily to cloud-top radiative cooling between 800 and 900 hPa, where cold air outbreaks in the warmer climate spend much of their time. Figure 8b demonstrates this effect with composites of cloud liquid and the vertical structure of the longwave temperature tendency along trajectories. In the warmer climate, cloud liquid peaks around 900 hPa and the longwave temperature tendency peaks along the top of the cloud layer between 800 and 850 hPa at values around 0.1 K/hr, or upwards of 2 K/day. In the pre-

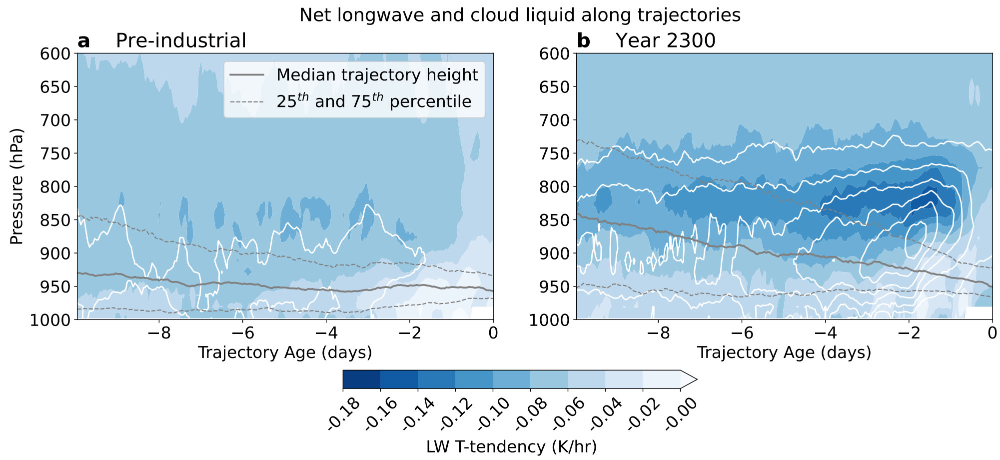

FIG. 8. Cloud-top radiative cooling enhances longwave diabatic cooling in the warmer climate scenario. Composites of the longwave temperature tendency (shaded contours) and cloud liquid (solid contours) profiles over all cold air outbreak trajectories in the pre-industrial (left) and year 2300 (right) model scenarios. Grey lines mark the median (solid) and 25^{th}–75^{th} percentile range (dashed) of trajectory heights across all trajectories. Cloud liquid contours start at 1×10^{-5} kg/kg and have a constant spacing of 1×10^{-5} kg/kg.

industrial climate, by contrast (Figure 8a), cloud liquid is almost an order of magnitude lower and the longwave temperature tendency does not vary much with height. The presence of thicker liquid clouds, made possible by higher temperatures and moisture in the warmer climate, increases longwave radiative cooling within the boundary layer and is responsible for more intense longwave radiative cooling along cold air outbreak trajectories.

4. Discussion and Conclusions

Wintertime cold air outbreaks affect large swathes of the interior of North America, but their behavior under global warming has proven challenging to predict. In spite of the mean warming trend over the last few decades and its amplification in the Arctic, there is disagreement on whether cold air outbreaks have declined as well. We know that warming wins out eventually, because warmer paleoclimate periods like the Eocene (56–34 Mya) present fossil evidence of strong suppression of cold extremes over continental interiors. Therefore, a better understanding of the mechanisms that sustain or suppress cold extremes in a variety of climate states could bolster our knowledge of paleoclimates and improve predictions of temperature extremes under future warming.

In this study, we analyze the development of North American wintertime cold air outbreaks using the Community Earth System Model, CESM2. We compare two climate scenarios with prescribed greenhouse gases, sea surface temperature, and sea ice coverage, corresponding to a pre-industrial case and a high-emissions case circa the year 2300, which produces Eocene-like conditions. A mid-latitude cold air outbreak may involve some combination of cold initial temperatures in the source region and cooling along the path of travel due to diabatic effects, so we consider both of these factors in our analysis. In the first half of the paper, we analyze climatological differences in cold air outbreak source regions between the pre-industrial and the much warmer climate scenario to quantify the availability of cold air. In the second half, we use a breakdown of the temperature tendencies due to distinct physics processes affecting air parcels as they travel into the mid-latitudes to clarify the role of diabatic heating and cooling in turning Arctic air masses into mid-latitude cold air outbreaks.

We began this paper by posing two key questions: given the persistence of North American cold air outbreaks observed over the last few decades in spite of an overall warming trend, when and why will they decline as warming continues? And how did much warmer past climates like the Eocene, which may serve as an analog for warmer future climates, so effectively suppress below-freezing temperatures over continental interiors? In the process of addressing these questions below, we highlight our three main results: (1) the latent heat of freezing suppresses warm extremes in a pre-industrial climate and cold extremes in a much warmer climate; (2) the transition to a warmer climate, and in particular the loss of Arctic sea ice and the near-surface temperature inversion at high latitudes, dramatically decreases the availability of below-freezing air, suppressing mid-latitude cold extremes; and (3) while the net diabatic temperature change along cold air outbreak trajectories is nearly identical between the pre-industrial and the much warmer climate, the primary heating and cooling mechanisms both get stronger in the warmer climate.

Based on wintertime temperature distributions over the interior of North America, we determined that the latent heat of freezing serves as a significant barrier to extreme temperatures in both climate scenarios. In a warmer climate, where wintertime surface temperatures are generally above freezing, liquid water in surface soils has the potential to release enough heat through freezing to offset the energy lost to surface sensible heat flux as a cold air mass approaches, preventing surface temperatures from dropping below freezing. The converse occurs in a cold climate, as ice near the surface can absorb excess heat through melting and resist the formation of above-freezing air. Both effects are visible in the sharp drop of the wintertime temperature distribution at freezing (Figure 1), shortening the warm tail of the pre-industrial distribution and suppressing below-freezing temperatures in the warmer climate. This result implies that the availability of surface and soil water can have an important mitigating effect on the development of temperature extremes near the freezing temperature.

The transition to a warmer climate is also accompanied by a marked decrease in the availability of below-freezing air in the Arctic source region, a result of changes to a handful of key climatological features. Increased heat fluxes from the ocean to the atmosphere at high latitudes (Figure 3), a result of the disappearance of Arctic sea ice in the warmer climate, raise surface temperatures over the Arctic Ocean above freezing, dramatically reducing the availability of below-freezing air near the surface (Figure 2). The near-surface temperature inversion, present throughout the winter at high latitudes in the pre-industrial climate, also disappears in the warmer climate (Figure 5), a manifestation of Arctic amplification. This removes the layer of stable, cold, dry air near the surface that supplied most of the cold air masses in the pre-industrial case. It also presents an avenue to predicting the decline of cold air outbreaks in the near future: Arctic sea ice and the near-surface temperature inversion are crucial to supplying the extremely cold air masses that can turn into mid-latitude cold air outbreaks. Disruptions to either of those features are likely to result in a significant shift in the availability of cold air masses.

Given the dramatic changes to temperature and stability in source regions that accompany the transition to a warmer climate, it is remarkable how little the dynamics and net diabatic effects were found to change. Cold air outbreak trajectories are less heavily clustered over the Arctic Ocean in the warmer climate relative to the pre-industrial case, but over half still pass over on their way to the mid-latitudes (Figure 4). The Arctic therefore continues to serve as the primary source region for cold air outbreaks. The net diabatic temperature change along trajectories is also nearly identical, at -6.5 K for the pre-industrial and -6.3 K for the warmer climate.

The similarity in net diabatic effect across the two climate scenarios would be surprising in its own right considering all of the changes to atmospheric temperature and moisture that accompany the shift to an Eocene-like climate, but is even more remarkable given the changes to two of the largest contributors to diabatic temperature change, longwave radiation and boundary layer mixing

(Figure 6). Longwave cooling is more intense in the warmer climate due to enhanced cloud-top radiative cooling (Figure 8), while warming from boundary layer mixing is also stronger and reflects more effective redistribution of enhanced surface sensible heat fluxes (Figure 7). While the net effect is the same for the pre-industrial and the warmer climate, the distribution of total physics temperature tendency is narrower (Figure 6d), which could reflect a greater correlation between the two competing effects via convection. This result also has implications for the challenges encountered by climate models attempting to represent cold air suppression in Eocene-like continental interiors. The enhancement of both the longwave and boundary layer mixing temperature tendencies in the warmer climate is primarily a result of cloud and convection processes, which are notoriously tricky to simulate. Models may be missing or misrepresenting key elements of these processes in the extreme conditions of a much warmer climate, where we have few modern analogs with which to develop and test parameterizations.

When considering the scope and implications of this work, it is important to keep in mind several caveats. We note that our warmer climate scenario, intended to emulate the year 2300 of an extended high-emissions run of CESM, is not a direct simulation of the Eocene itself but rather evocative of much warmer climates. By using a 2000-era model configuration as a starting point, we incorporate modern vegetation, land ice, and topography while setting greenhouse gases to match projected anthropogenic emissions. We chose these conditions in pursuit of a signal in the occurrence and characteristics of cold events that is strong enough to be differentiated from that of the pre-industrial scenario and to allow for attribution to changes in radiative forcing, sea ice, and sea surface temperature rather than variable vegetation and topographic effects, which we feel was largely successful. There are also limitations to the interpretability of our trajectory analysis, which are also discussed in detail in Hartig et al. (2023) but will be restated here. The diabatic temperature budget residual for a Lagrangian trajectory, which should be zero, is near zero for the majority of trajectories but upwards of 10 K for a handful in both climate scenarios (Figure 6e). We attribute these residuals (budget errors) primarily to the effect of vertical positioning errors in HYSPLIT that are further exaggerated by the strong vertical temperature gradients in near-surface winter-time inversions. This is consistent with the reduced error in the warmer climate scenario where vertical temperature gradients are smaller due to the loss of the near-surface temperature inversion. As the median residual for both scenarios is zero, our focus remains on the differences in temperature tendency between the two scenarios and the physical mechanisms we can identify that explain those differences. With our method, we are able to quantify the residual itself rather than attributing it to a collection of physical processes that do not have an explicit temperature tendency as is more commonly done.

Ultimately, we have developed a mechanistic understanding of North American cold air outbreaks and how they might change in a warmer climate. Both the availability of cold air in high-latitude source regions and diabatic effects acting to heat or cool air masses as they travel into the mid-latitudes can affect the development of wintertime cold extremes. The median diabatic cooling is -6 K for air parcels traveling toward cold events. But it ranges into tens of degrees for many trajectories, so diabatic effects often play a major role in the evolution of Arctic air masses in both the pre-industrial and the much warmer climate scenario. Since the net diabatic effect is the same in the two scenarios, we find that the decreased availability of cold air in the Arctic in a warmer climate is sufficient to suppress below-freezing temperatures over the interior of North America in spite of the persistence of diabatic cooling along air parcel trajectories in the warmer climate scenario. To understand and predict changes to cold air outbreaks in a warming world, we must therefore account for changes to both source regions and diabatic processes, as either can tip the scale in controlling whether an Arctic air mass becomes a cold air outbreak when swept into the mid-latitudes.

Acknowledgments. This work was funded by NSF grant 2303486 from the P4CLIMATE program. KH is funded by a National Defense Science and Engineering Graduate (NDSEG) Fellowship. ET thanks the Weizmann Institute for its hospitality during parts of this work. Computing and data storage resources, including the Cheyenne supercomputer (doi:10.5065/D6RX99HX), were provided by the Computational and Information Systems Laboratory (CISL) at NCAR. NCAR is sponsored by the National Science Foundation. Special thanks to Brian Medeiros for help with the CAM6 temperature budget and setting up fixed GHG runs in CESM2, and to Adam Herrington for a breakdown of the processes covered by CLUBB in CAM6.

Data availability statement. Simulations were performed using CESM2.1.3 with CAM6, which is freely available at `https://www.cesm.ucar.edu/models/cesm2` following registration. The CESM2-WACCM output used to generate prescribed SST and sea ice files for the Year 2300 scenario is available at `http://doi.org/10.22033/ESGF/CMIP6.10115` under the ssp585 tag. Fixed greenhouse gas concentrations for the Year 2300 scenario come from Meinshausen et al. (2020). Back trajectories were calculated using HYSPLIT v5.1.0 (with modifications described in Hartig et al. (2023)), which is freely available at `https://www.ready.noaa.gov/HYSPLIT.php`. Code used to interpolate CAM data onto HYSPLIT trajectories is available on GitHub at `https://github.com/kahartig/camtrack`.

References

Abu-Hamdeh, N. H., 2003: Thermal Properties of Soils as affected by Density and Water Content. *Biosystems Engineering*, **86 (1)**, 97–102, https://doi.org/10.1016/S1537-5110(03)00112-0.

Arias, P. A., and Coauthors, 2021: Technical summary. *Climate Change 2021: The Physical Science Basis. Contribution of Working Group I to the Sixth Assessment Report of the Intergovernmental Panel on Climate Change*, V. Masson-Delmotte, P. Zhai, A. Pirani, S. L. Connors, C. Péan, S. Berger, N. Caud, Y. Chen, L. Goldfarb, M. I. Gomis, M. Huang, K. Leitzell, E. Lonnoy, J. B. R. Matthews, T. K. Maycock, T. Waterfield, Ö. Yelekçi, R. Yu, and B. Zhou, Eds., Cambridge University Press.

Beerling, D. J., and D. L. Royer, 2011: Convergent Cenozoic CO2 history. *Nature Geoscience*, **4 (7)**, 418–420, https://doi.org/10.1038/ngeo1186.

Bogenschutz, P. A., A. Gettelman, H. Morrison, V. E. Larson, C. Craig, and D. P. Schanen, 2013: Higher-Order Turbulence Closure and Its Impact on Climate Simulations in the Community Atmosphere Model. *Journal of Climate*, **26 (23)**, 9655–9676, https://doi.org/10.1175/JCLI-D-13-00075.1.

Caballero, R., and M. Huber, 2013: State-dependent climate sensitivity in past warm climates and its implications for future climate projections. *Proceedings of the National Academy of Sciences*, **110 (35)**, 14 162–14 167, https://doi.org/10.1073/pnas.1303365110.

Cellitti, M. P., J. E. Walsh, R. M. Rauber, and D. H. Portis, 2006: Extreme cold air outbreaks over the United States, the polar vortex, and the large-scale circulation. *Journal of Geophysical Research: Atmospheres*, **111 (D2)**, https://doi.org/10.1029/2005JD006273.

Cohen, J., and D. Entekhabi, 1999: Eurasian snow cover variability and northern hemisphere climate predictability. *Geophysical Research Letters*, **26 (3)**, 345–348, https://doi.org/10.1029/1998GL900321.

Cohen, J., and Coauthors, 2014: Recent Arctic amplification and extreme mid-latitude weather. *Nature Geoscience*, **7 (9)**, 627–637, https://doi.org/10.1038/ngeo2234.

Cronin, T. W., and E. Tziperman, 2015: Low clouds suppress Arctic air formation and amplify high-latitude continental winter warming. *Proceedings of the National Academy of Sciences*, **112 (37)**, 11 490–11 495, https://doi.org/10.1073/pnas.1510937112.

Draxler, R. R., 1999: HYSPLIT 4 User's Guide. NOAA Tech. Rep. ERL ARL-230, NOAA/Air Resources Laboratory, 38 pp.

Draxler, R. R., and G. D. Hess, 1997: Description of the HYSPLIT 4 modeling system. NOAA Tech. Rep. ERL ARL-224, NOAA/Air Resources Laboratory, 31 pp.

Draxler, R. R., and G. D. Hess, 1998: An Overview of the HYSPLIT_4 Modelling System for Trajectories, Dispersion, and Deposition. *Australian Meteorological Magazine*, 295–308.

Ellis, A. W., and D. J. Leathers, 1998: A Quantitative Approach to Evaluating the Effects of Snow Cover on Cold Airmass Temperatures across the U.S. Great Plains. *Weather and Forecasting*, **13 (3)**, 688–701, https://doi.org/10.1175/1520-0434(1998)013⟨0688:AQATET⟩2.0.CO;2.

Gao, Y., L. R. Leung, J. Lu, and G. Masato, 2015: Persistent cold air outbreaks over North America in a warming climate. *Environmental Research Letters*, **10 (4)**, 044 001, https://doi.org/10.1088/1748-9326/10/4/044001.

Golaz, J.-C., V. E. Larson, and W. R. Cotton, 2002: A PDF-Based Model for Boundary Layer Clouds. Part I: Method and Model Description. *Journal of the Atmospheric Sciences*, **59 (24)**, 3540–3551, https://doi.org/10.1175/1520-0469(2002)059⟨3540:APBMFB⟩2.0.CO;2.

Gong, G., D. Entekhabi, and J. Cohen, 2003: Modeled Northern Hemisphere Winter Climate Response to Realistic Siberian Snow Anomalies. *Journal of Climate*, **16 (23)**, 3917–3931, https://doi.org/10.1175/1520-0442(2003)016⟨3917:MNHWCR⟩2.0.CO;2.

Greenwood, D. R., and S. L. Wing, 1995: Eocene continental climates and latitudinal temperature gradients. *Geology*, **23 (11)**, 1044–1048, https://doi.org/10.1130/0091-7613(1995)023⟨1044:ECCALT⟩2.3.CO;2.

Grotjahn, R., and Coauthors, 2016: North American extreme temperature events and related large scale meteorological patterns: a review of statistical methods, dynamics, modeling, and trends. *Climate Dynamics*, **46 (3)**, 1151–1184, https://doi.org/10.1007/s00382-015-2638-6.

Hankes, I. E., and J. E. Walsh, 2011: Characteristics of extreme cold air masses over the North American sub-Arctic. *Journal of Geophysical Research: Atmospheres*, **116 (D11)**, https://doi.org/10.1029/2009JD013582.

Hartig, K., E. Tziperman, and C. P. Loughner, 2023: Processes Contributing to North American Cold Air Outbreaks Based on Air Parcel Trajectory Analysis. *Journal of Climate*, **36 (3)**, 931–943, https://doi.org/10.1175/JCLI-D-22-0204.1.

Heinemann, M., J. H. Jungclaus, and J. Marotzke, 2009: Warm Paleocene/Eocene climate as simulated in. *Clim. Past*, 18.

Huber, M., and R. Caballero, 2011: The early Eocene equable climate problem revisited. *Climate of the Past*, **7 (2)**, 603–633, https://doi.org/10.5194/cp-7-603-2011.

Hurrell, J. W., J. J. Hack, D. Shea, J. M. Caron, and J. Rosinski, 2008: A New Sea Surface Temperature and Sea Ice Boundary Dataset for the Community Atmosphere Model. *Journal of Climate*, **21 (19)**, 5145–5153, https://doi.org/10.1175/2008JCLI2292.1.

Hutchison, J. H., 1982: Turtle, crocodilian, and champsosaur diversity changes in the Cenozoic of the north-central region of western United States. *Palaeogeography, Palaeoclimatology, Palaeoecology*, **37 (2)**, 149–164, https://doi.org/10.1016/0031-0182(82)90037-2.

Hyland, E. G., K. W. Huntington, N. D. Sheldon, and T. Reichgelt, 2018: Temperature seasonality in the North American continental interior during the Early Eocene Climatic Optimum. *Climate of the Past*, **14 (10)**, 1391–1404, https://doi.org/10.5194/cp-14-1391-2018.

Inglis, G. N., and Coauthors, 2020: Global mean surface temperature and climate sensitivity of the early Eocene Climatic Optimum (EECO), Paleocene–Eocene Thermal Maximum (PETM), and latest Paleocene. *Climate of the Past*, **16 (5)**, 1953–1968, https://doi.org/10.5194/cp-16-1953-2020.

Kolstad, E. W., T. Breiteig, and A. A. Scaife, 2010: The association between stratospheric weak polar vortex events and cold air outbreaks in the Northern Hemisphere. *Quarterly Journal of the Royal Meteorological Society*, **136 (649)**, 886–893, https://doi.org/10.1002/qj.620.

Liu, J., J. A. Curry, H. Wang, M. Song, and R. M. Horton, 2012: Impact of declining Arctic sea ice on winter snowfall. *Proceedings of the National Academy of Sciences*, **109 (11)**, 4074–4079, https://doi.org/10.1073/pnas.1114910109.

Lunt, D. J., and Coauthors, 2012: A model–data comparison for a multi-model ensemble of early Eocene atmosphere–ocean simulations: EoMIP. *Climate of the Past*, **8 (5)**, 1717–1736, https://doi.org/10.5194/cp-8-1717-2012.

Markwick, P. J., 1994: "Equability," continentality, and Tertiary "climate": The crocodilian perspective. *Geology*, **22 (7)**, 613–616, https://doi.org/10.1130/0091-7613(1994)022⟨0613:ECATCT⟩2.3.CO;2.

Markwick, P. J., 1998: Fossil crocodilians as indicators of Late Cretaceous and Cenozoic climates: implications for using palaeontological data in reconstructing palaeoclimate. *Palaeogeography, Palaeoclimatology, Palaeoecology*, **137 (3)**, 205–271, https://doi.org/10.1016/S0031-0182(97)00108-9.

Meinshausen, M., and Coauthors, 2020: The shared socio-economic pathway (SSP) greenhouse gas concentrations and their extensions to 2500. *Geoscientific Model Development*, **13 (8)**, 3571–3605, https://doi.org/10.5194/gmd-13-3571-2020.

NWS, 2023: Nowdata climate for western and central wyoming. NOAA/National Weather Service, accessed 10 Aug 2023, https://www.weather.gov/wrh/Climate?wfo=riw.

Oldenborgh, G. J. v., E. Mitchell-Larson, G. A. Vecchi, H. d. Vries, R. Vautard, and F. Otto, 2019: Cold waves are getting milder in the northern midlatitudes. *Environmental Research Letters*, **14 (11)**, 114 004, https://doi.org/10.1088/1748-9326/ab4867.

Portis, D. H., M. P. Cellitti, W. L. Chapman, and J. E. Walsh, 2006: Low-Frequency Variability and Evolution of North American Cold Air Outbreaks. *Monthly Weather Review*, **134 (2)**, 579–597, https://doi.org/10.1175/MWR3083.1.

Robeson, S. M., C. J. Willmott, and P. D. Jones, 2014: Trends in hemispheric warm and cold anomalies. *Geophysical Research Letters*, **41 (24)**, 9065–9071, https://doi.org/https://doi.org/10.1002/2014GL062323.

Screen, J. A., 2014: Arctic amplification decreases temperature variance in northern mid- to high-latitudes. *Nature Climate Change*, **4 (7)**, 577–582, https://doi.org/10.1038/nclimate2268.

Shellito, C. J., L. C. Sloan, and M. Huber, 2003: Climate model sensitivity to atmospheric CO2 levels in the Early–Middle Paleogene. *Palaeogeography, Palaeoclimatology, Palaeoecology*, **193 (1)**, 113–123, https://doi.org/10.1016/S0031-0182(02)00718-6.

Smith, E. T., and S. C. Sheridan, 2018: The characteristics of extreme cold events and cold air outbreaks in the eastern United States. *International Journal of Climatology*, **38 (S1)**, e807–e820, https://doi.org/https://doi.org/10.1002/joc.5408.

Smith, E. T., and S. C. Sheridan, 2020: Where Do Cold Air Outbreaks Occur, and How Have They Changed Over Time? *Geophysical Research Letters*, **47 (13)**, e2020GL086 983, https://doi.org/https://doi.org/10.1029/2020GL086983.

Stein, A. F., R. R. Draxler, G. D. Rolph, B. J. B. Stunder, M. D. Cohen, and F. Ngan, 2015: NOAA's HYSPLIT Atmospheric Transport and Dispersion Modeling System. *Bulletin of the American Meteorological Society*, **96 (12)**, 2059–2077, https://doi.org/10.1175/BAMS-D-14-00110.1.

Vavrus, S., 2007: The role of terrestrial snow cover in the climate system. *Climate Dynamics*, **29 (1)**, 73–88, https://doi.org/10.1007/s00382-007-0226-0.

Vavrus, S., J. E. Walsh, W. L. Chapman, and D. Portis, 2006: The behavior of extreme cold air outbreaks under greenhouse warming. *International Journal of Climatology*, **26 (9)**, 1133–1147, https://doi.org/10.1002/joc.1301.

Vavrus, S. J., F. Wang, J. E. Martin, J. A. Francis, Y. Peings, and J. Cattiaux, 2017: Changes in North American Atmospheric Circulation and Extreme Weather: Influence of Arctic Amplification and Northern Hemisphere Snow Cover. *Journal of Climate*, **30 (11)**, 4317–4333, https://doi.org/10.1175/JCLI-D-16-0762.1.

Walsh, J. E., A. S. Phillips, D. H. Portis, and W. L. Chapman, 2001: Extreme Cold Outbreaks in the United States and Europe, 1948–99. *Journal of Climate*, **14 (12)**, 2642–2658, https://doi.org/10.1175/1520-0442(2001)014⟨2642:ECOITU⟩2.0.CO;2.

Westby, R. M., Y.-Y. Lee, and R. X. Black, 2013: Anomalous Temperature Regimes during the Cool Season: Long-Term Trends, Low-Frequency Mode Modulation, and Representation in CMIP5 Simulations. *Journal of Climate*, **26 (22)**, 9061–9076, https://doi.org/10.1175/JCLI-D-13-00003.1.

Wing, S. L., and D. R. Greenwood, 1993: Fossils and Fossil Climate: The Case for Equable Continental Interiors in the Eocene. *Philosophical Transactions: Biological Sciences*, **341 (1297)**, 243–252.

Zhu, J., C. J. Poulsen, and J. E. Tierney, 2019: Simulation of Eocene extreme warmth and high climate sensitivity through cloud feedbacks. *Science Advances*, **5 (9)**, eaax1874, https://doi.org/10.1126/sciadv.aax1874.